Cell Reports

The Histone Methyltransferase G9a Controls Axon Growth by Targeting the RhoA Signaling Pathway

Graphical Abstract

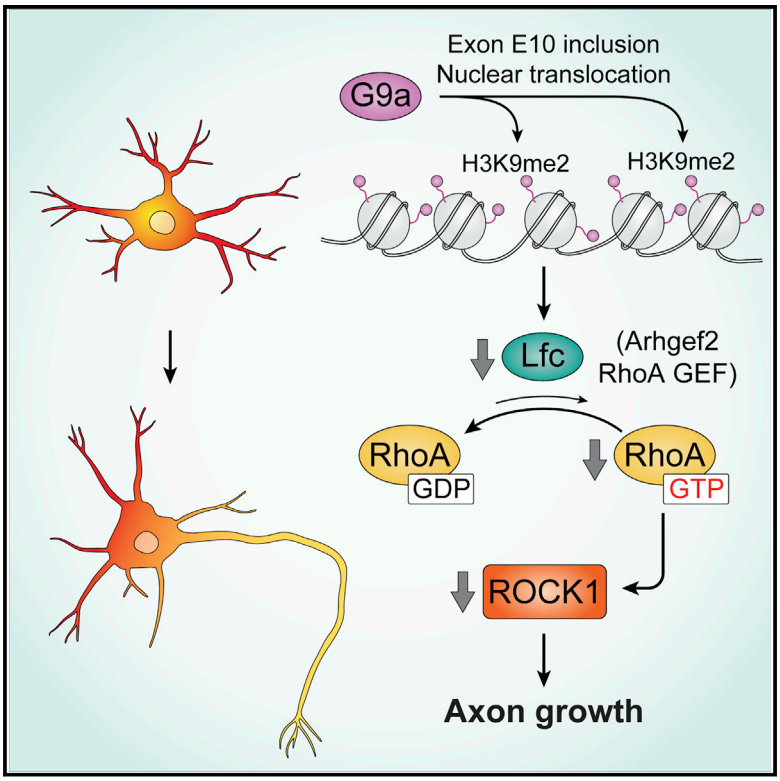

Authors

Carlos Wilson, Luciana E. Giono, Victoria Rozés-Salvador, Ana Fiszbein, Alberto R. Kornblihtt, Alfredo Cáceres

Correspondence

acaceres@immf.uncor.edu

In Brief

Wilson et al. report that G9a allows the establishment of neuronal polarity, axon growth, and neuronal cortical migration. Through a H3K9me2-dependent mechanism, G9a regulates the expression of Lfc, a RhoGEF that promotes RhoA/ROCK signaling. This report links histone methylation with neuronal polarization and axonal development.

Highlights

- G9a expression and nuclear enrichment occur early in polarizing neurons
- G9a is required for neuronal migration and axon formation
- G9a inhibits RhoA/ROCK activity during neuronal polarization
- G9a targets Lfc, a GEF for RhoA that impairs axon growth

Wilson et al., 2020, Cell Reports *31*, 107639
May 12, 2020
https://doi.org/10.1016/j.celrep.2020.107639

CellPress

Cell Reports

CellPress
OPEN ACCESS

Report

The Histone Methyltransferase G9a Controls Axon Growth by Targeting the RhoA Signaling Pathway

Carlos Wilson,[1,2,3] Luciana E. Giono,[4] Victoria Rozés-Salvador,[1,2] Ana Fiszbein,[4] Alberto R. Kornblihtt,[4] and Alfredo Cáceres[1,2,3,5,*]

[1]Instituto de Investigación Médica Mercedes y Martín Ferreyra (INIMEC-CONICET-UNC) Friuli 2434, 5016 Córdoba, Argentina
[2]Universidad Nacional de Córdoba (UNC), Av. Haya de la Torre s/n, 5000 Córdoba, Argentina
[3]Centro de Investigación en Medicina Traslacional "Severo R Amuchástegui" (CIMETSA), Instituto Universitario Ciencias Biomédicas Córdoba (IUCBC), Av. Friuli 2786, 5016 Córdoba, Argentina
[4]Instituto de Fisiología, Biología Molecular y Neurociencias (IFIBYNE-UBA-CONICET) and Departamento de Fisiología, Biología Molecular y Celular, Facultad de Ciencias Exactas y Naturales, Universidad de Buenos Aires, Ciudad Universitaria, C1428EHA Buenos Aires, Argentina
[5]Lead Contact
*Correspondence: acaceres@immf.uncor.edu
https://doi.org/10.1016/j.celrep.2020.107639

SUMMARY

The generation of axonal and dendritic domains is critical for brain circuitry assembly and physiology. Negative players, such as the RhoA-Rho coiled-coil-associated protein kinase (ROCK) signaling pathway, restrain axon development and polarization. Surprisingly, the genetic control of neuronal polarity has remained largely unexplored. Here, we report that, in primary cultured neurons, expression of the histone methyltransferase G9a and nuclear translocation of its major splicing isoform (G9a/E10+) peak at the time of axon formation. RNAi suppression of G9a/E10+ or pharmacological blockade of G9a constrains neuronal migration, axon initiation, and the establishment of neuronal polarity *in situ* and *in vitro*. Inhibition of G9a function upregulates RhoA-ROCK activity by increasing the expression of Lfc, a guanine nucleotide exchange factor (GEF) for RhoA. Together, these results identify G9a as a player in neuronal polarization.

INTRODUCTION

The regulation of gene expression is critical to supply products demanded by developing neurons. In this regard, epigenetics enclose different aspects of gene regulation, including DNA and histone modifications that reshape chromatin in response to transcriptional requirements (Hwang et al., 2017). Histone post-translational modifications contribute to shape chromatin structure, switching between transcriptionally active and inactive states (Gardner et al., 2011; Hwang et al., 2017; Tan et al., 2011). Accordingly, the histone methyltransferase G9a catalyzes the dimethylation of H3K9 (H3K9me2), considered a repressive mark (Mozzetta et al., 2014; Roopra et al., 2004; Shinkai and Tachibana, 2011; Tachibana et al., 2002; Tachibana et al., 2008). Recent reports have linked G9a with neuronal functions, including neurogenesis (Kim et al., 2016; Olsen et al., 2016), neurite growth (Fiszbein et al., 2016; Fiszbein and Kornblihtt, 2016), synaptic plasticity (Sharma et al., 2017a, 2017b; Sharma and Sajikumar, 2019), and neurodegeneration (Liang et al., 2016a, 2016b). However, the contribution of G9a to early neuronal development, including axon/dendrite differentiation and growth, is missing.

A critical step in the early life of neurons is the acquisition of polarity, where axonal and dendritic domains are generated (Barnes and Polleux, 2009; Cáceres et al., 2012). A wide variety of factors have been identified as key regulators of cytoskeletal organization and dynamics required for neuronal polarization (Bradke and Dotti, 1997; Namba et al., 2015; Stiess and Bradke, 2011). Nevertheless, genetic mechanisms controlling cytoskeleton organization and its contribution to the acquisition of neuronal polarity have remained largely unexplored.

We now describe a mechanism controlling the activity of the RhoA pathway, a critical regulator of axon initiation and growth (Dupraz et al., 2019). Using *in vivo* and *in vitro* approaches, we report that basal activity of G9a is required for axon growth and cortical migration of neurons. We have detected that G9a targets Lfc expression, a guanine exchange factor (GEF) for RhoA, and hence the activity of the RhoA/Rho coiled-coil-associated protein kinase (ROCK) signaling pathway, a key constraint for axon growth during polarization.

RESULTS

G9a Is Expressed Early in Polarizing Neurons

We evaluated G9a expression and distribution in cultured hippocampal neurons within the first 72 h *in vitro*, a time period in which polarization is defined in this model system (Figures 1A–1C). G9a immunofluorescence was detected in neurons at the time of plating, displaying both cytoplasmic and nuclear localization; within the next 72 h, a progressive increase in its nuclear

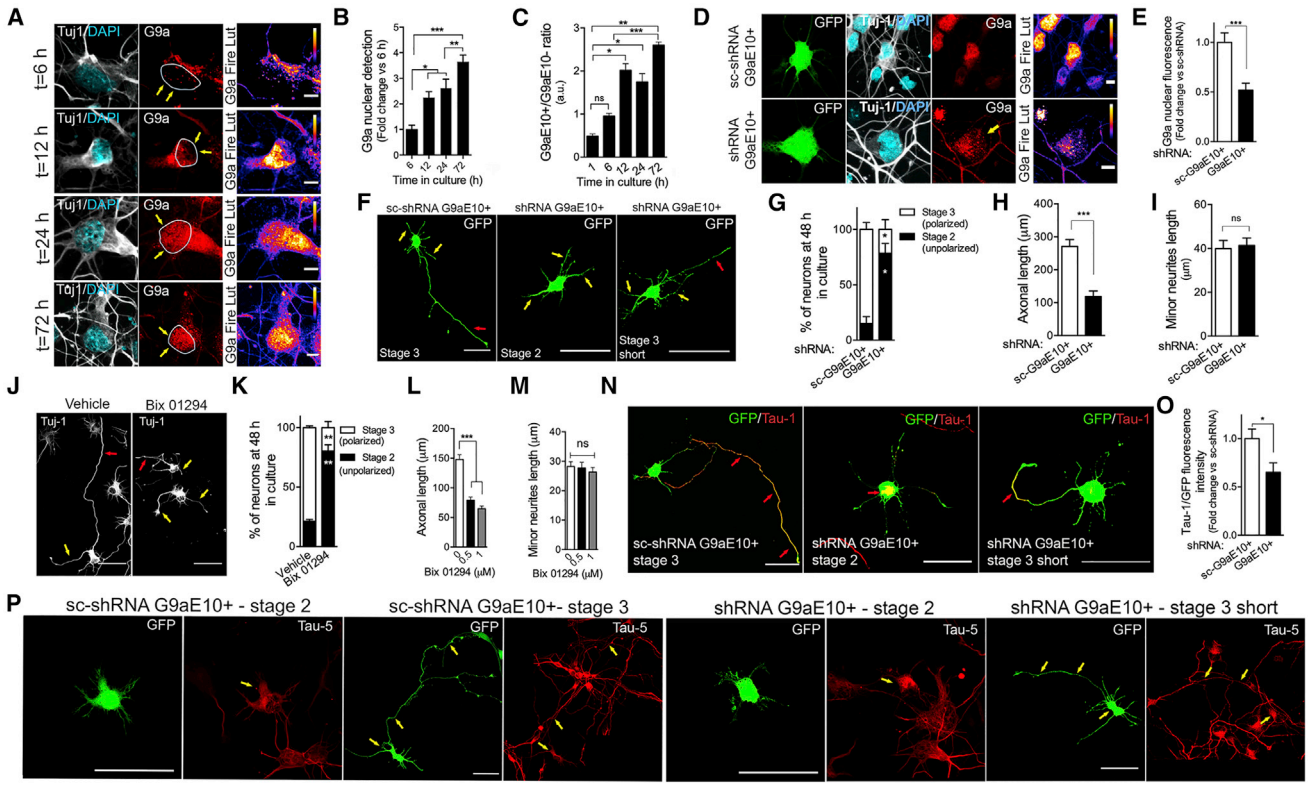

Figure 1. G9a/E10+ Is Required for Neuronal Polarity and Axon Growth in Cultured Neurons

(A) Images showing G9a (red) distribution by immunofluorescence (IF) in cultured neurons at different times after plating (6–72 h). Nuclei (blue) were labeled with DAPI. Fire (lookup table) LUT corresponds to G9a IF.

(B) Quantification of nuclear G9a IF (normalized by DAPI; for experimental details, see Method Details).

(C) Quantification of G9a/E10+ to G9a/E10− ratio by radioactive RT-PCR in cultured neurons (1–72 h).

(D) Images showing neurons transfected shortly after plating with shRNA-G9a/E10+/GFP or sc-shRNAG9a/E10+/GFP (control) and fixed at 2 DIV (days *in vitro*). Neurons were stained to detect G9a (red), TuJ1 (white), and DAPI (blue) by IF.

(E) Quantification of knockdown efficiency of G9a by IF (see experimental details in Method Details).

(F) Representative control and shRNA-G9a/E10+/GFP-expressing neurons at 2 DIV.

(G) Quantification (%) of stages 2 and 3 neurons at 2 DIV.

(H and I) Quantification of average axonal (H) and minor neurite (I) lengths.

(J–M) (J) Representative images of neurons treated with Bix 01294 after plating and fixed at 2 DIV. (K) Quantification (%) of stages 2 and 3 neurons and axonal (L) and minor neurite lengths (M) at 2 DIV after 1 µM Bix 01294 treatment.

(N) Tau-1 IF in control and shRNA-G9a/E10+/GFP neurons (2 DIV).

(O) Quantification of Tau-1 IF intensity (normalized by GFP emission).

(P) Total Tau detection by Tau-5 mAb IF in 2 DIV control or shRNA-G9a/E10+/GFP neurons (transfected after plating).

Graphs represent mean ± SEM. *$p < 0.05$, **$p < 0.01$, ***$p < 0.001$. Kruskal-Wallis test, multiple comparison (except in B and C; Student's t test). In total, 35–45 transfected neurons were analyzed for each condition from three independent cultures (n = 3). Scale bars: (A–D) 5 µm; (F–P) 50 µm.

localization became quite evident, paralleled by a decrease in the cytoplasmic staining (Figures 1A and 1B). Recently, we reported that in neuroblastoma cells, the alternative splicing isoform of G9a including exon 10 (G9a/E10+) is required for neurite outgrowth (Fiszbein et al., 2016). Therefore, it became of interest to evaluate expression of G9a/E10+ in cultured hippocampal neurons during the establishment of polarity.

To address this, we performed radioactive RT-PCR assays to estimate the G9a/E10+ to G9a/E10− mRNA ratio in extracts of neurons cultured from different time periods. The results obtained showed a progressive enrichment in G9a/E10+, which became evident as soon as 12 h after plating and remained high for at least 2 more days (Figure 1C); together, these observations suggest that G9a/E10+ is the main splicing variant in polarizing neurons and prompted us to evaluate the consequences of its suppression on axon formation. To this end, we designed a small hairpin RNA (shRNA) targeting a sequence within exon 10 of G9a mRNA to specifically knockdown the expression of G9a/E10+ (Figures 1D and 1E). Neurons were transfected immediately after plating with a pCAGIG-GFP plasmid, encoding shRNA-G9a/E10+, scrambled shRNA (sc-shRNA), or shRNA-luciferase. Immunofluorescence revealed a significant reduction of G9a staining 48 h after transfection of shRNA-G9a/E10+/GFP (Figure 1E), evident by the loss of nuclear staining (Figure 1D, lower panel arrows). A weak cytoplasmic signal remained, probably reporting the presence of the

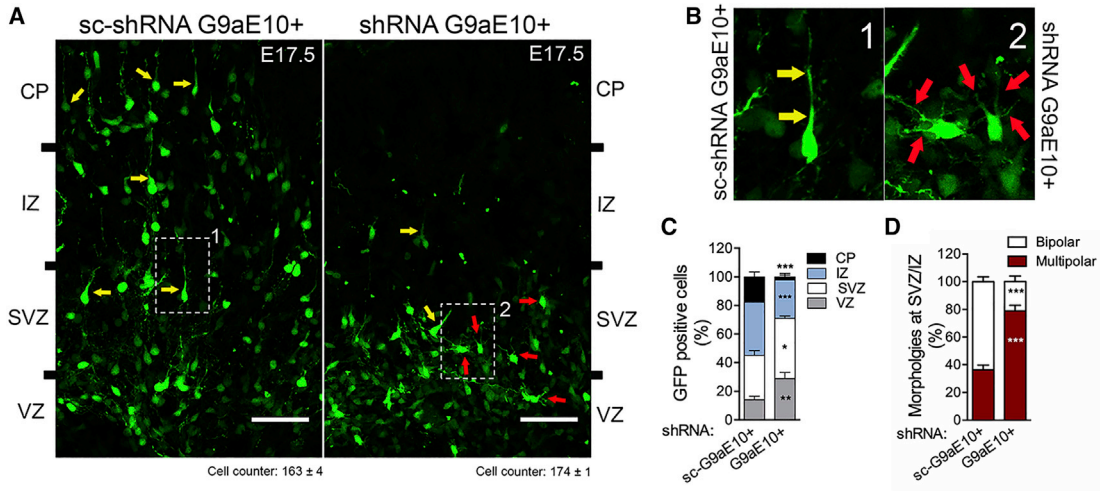

Figure 2. G9a/E10+ Allows Cortical Migration and Polarization *In Situ*

(A) Representative E17.5 coronal cortical slices of mouse brains expressing sc-shRNA (control) or shRNA-G9a/E10+/GFP after IUE (E15.5–E17-5).

(B) Magnification of insets 1 and 2 shown in (A).

(C) Quantification (%) of neurons by layer. VZ, ventricular zone; SVZ, subventricular zone; IZ, intermediate zone; CP, cortical plate.

(D) Estimation (%) of bipolar-multipolar cells at SVZ-IZ.

Graphs represent mean ± SEM. *p < 0.05, **p < 0.01, ***p < 0.001, Student's t test. In total, 8–12 slices were analyzed from three independent IUE experiments by each condition (n = 3), and 100–200 cells were counted by slice. Scale bar: 200 μm.

less-abundant splicing variant (G9a/E10−) unaffected by the knockdown of G9a/E10+. Besides, neurons expressing shRNA-G9a/E10+ showed a ~50% reduction of H3K9me2 (Figure S1), suggesting this mark is mainly catalyzed by G9a/E10+ in polarizing neurons.

G9a/E10+ Is Required for Axon Formation

In the following series of experiments, we evaluated the impact of G9a/E10+ suppression on the establishment of morphological polarity (i.e., extension of an axon). Neurons were transfected shortly after plating with either shRNA-G9a/E10+/GFP or sc-shRNA-G9a/E10+/GFP and fixed 48 h later to evaluate axon formation (Figures 1F–1H). As in previous work (Conde et al., 2010), a neurite was considered an axon if its length was at least 100 μm and/or 2–3 times longer than minor neurites of the same cell. By 2 days *in vitro* (DIV), more than 85% of control neurons have acquired morphological polarity (stage 3), exhibiting a single axon-like neurite and several shorter minor processes (Figures 1F and 1G). By contrast, almost 80% of shRNA-G9a/E10+ GFP-expressing neurons were arrested at stage 2 of polarity (i.e., neurons with a symmetric array of short neurites) (Figures 1F and 1G). A small percentage (less than 20%) was able to reach stage 3 but displayed short axon-like neurites (Figures 1F–1I). To complement these experiments, cultured neurons were treated with Bix 01294, a small molecule that blocks G9a catalytic activity (Kim et al., 2016; Kubicek et al., 2007; Sharma et al., 2017b); this treatment reproduced the phenotype observed after G9a/E10+ suppression (Figures 1J–1M).

The expression and distribution of a well-characterized axonal marker in control and G9a-suppressed neurons were also evaluated. A gradient of dephosphorylated Tau, selectively labeled by the Tau-1 mAb (Binder et al., 1985) and enriched toward the distal axon, has been extensively used as a canonical molecular marker for nascent and mature axons (Mandell and Banker, 1996). Very little Tau-1 IF signal was found in neurites from stage 2 neurons either in control or shRNA-G9a/E10+-treated cultures (Figure 1N). By contrast, while a well-defined Tau-1 gradient was found in axons from stage 3 sc-shRNA-G9a/E10+/GFP-treated neurons, the few shRNA-G9a/E10+/GFP neurons bearing a short axon showed faint Tau-1 signal (Figures 1N and 1O), despite no significant changes in total Tau as revealed by staining with the Tau-5 mAb (Figure 1P); a similar phenomenon was observed after Bix-01294 treatment (not shown).

Then, we evaluated the contribution of G9a to neuronal development *in situ*. To this end, *in utero* electroporation (IUE) of embryonic mouse brains (E15.5) with the pCAGIG-GFP plasmid encoding shRNA-G9a/E10+ was used to assess the consequences of G9a downregulation on cortical migration and polarization (Figure 2). Two days after IUE (E17.5), embryos were sacrificed, and GFP-expressing brains were fixed to visualize the cerebral cortex. Cortical migration was evaluated according to Kriegstein and Noctor (2004). Of note, we chose E15.5–E17.5 because within this time frame, migrating neurons undergo morphological transformations similar to the stage 2–3 transition observed *in vitro*.

For morphometric purposes, the embryonic cerebral cortex was divided in four layers: the ventricular zone (VZ), subventricular zone (SVZ), intermediate zone (IZ), and cortical plate (CP) (Fuentes et al., 2012). Figure 2A shows representative E17.5 coronal slices from sc-shRNA-G9a/E10+/GFP- and shRNA-G9a/E10+/GFP-expressing neurons. The results obtained showed that most shRNA-G9a/E10+/GFP-expressing cells failed to migrate and reach either the IZ or CP zones (Figures 2A and 2C).

Most neurons located at the SVZ display a multipolar phenotype, resembling the stage 2 of polarity observed in culture (Barnes and Polleux, 2009), while those located at the SVZ-IZ boundary display a bipolar morphology (Hatanaka and Yamauchi, 2013; Kriegstein and Noctor, 2004; Nakamuta et al., 2011). Therefore, we estimated the percentage of multipolar and bipolar neurons at SVZ-IZ zones in sc-shRNA and shRNA-G9a/E10+/GFP-treated animals. (Figures 2A, 2B, and 2D). Figure 2B shows representative bipolar and multipolar morphologies detected in control and G9a-suppressed neurons (insets 1 and 2, respectively). As expected, 64% of control neurons had bipolar morphologies, characteristic of polarized neurons (Figures 2B and 2D). However, 79% of shRNA-G9a/E10+/GFP-expressing neurons displayed a multipolar phenotype, resembling the one observed after G9a/E10+ suppression in culture. Together, our data suggest that G9a/E10+ is instrumental for axon growth initiation and morphological polarization.

The RhoA Pathway Is Targeted by G9a in Developing Neurons

To explore a possible mechanism underlying G9a participation in axon formation, we hypothesized that G9a might repress the expression of inhibitors of polarization, such as members of the RhoA/ROCK pathway. We based our hypothesis on the following evidence. First, downregulation of RhoA-ROCK is required for axon formation (Conde et al., 2010; Xu et al., 2015; Takano et al., 2017; Dupraz et al., 2019). Second, phosphorylation of Tau partially depends on ROCK (Amano et al., 2003), decreasing Tau-1 immunoreactivity (Mandell and Banker, 1996). Finally, G9a controls ROCK expression in non-neuronal cells (Bian et al., 2015).

To begin testing this idea, we first measured RhoA and ROCK activities using Förster Resonance Energy Transfer (FRET) in neurons expressing genetically encoded biosensors. Hippocampal cultures were transfected immediately after plating with a RhoA biosensor designated as RhoA1G (Fritz et al., 2013)—or Eevee-ROCK, a biosensor based on the Eevee backbone carrying the consensus substrate sequence for ROCK (Li et al., 2017)—to measure RhoA and ROCK activities by FRET using ratio imaging, respectively (Quassollo et al., 2015). To achieve an acute and fast loss of G9a function, neurons were treated with Bix 01294 immediately after transfection and fixed 18 h later. We focused our analyses on neurons showing a nascent axon in both control and G9a-inhibited conditions; then, we analyzed FRET efficiencies in the axon, minor neurites, and soma (Figures 3A–3N). Treatment with Bix 01294 significantly increased RhoA and ROCK activities in the axonal compartment (Figures 3A–3N), suggesting that G9a controls RhoA/ROCK activities in polarizing neurons.

We then evaluated whether ROCK inhibition could rescue axonal growth defects in G9a/E10+-suppressed neurons. To this end, control or shRNA-G9a/E10+/GFP-transfected neurons were treated with Y-27632 (10 μM), a specific inhibitor of ROCK1/2 (Darenfed et al., 2007) (Figures 3O, 3Q, and 3R). The results obtained showed that Y-27632 rescues the phenotype after silencing G9a/E10+, with most neurons developing a Tau-1+ axon-like neurite (Figure 3O). A similar effect was observed in neurons treated with Bix 01294 (Figures 3P, 3S, and 3T). Together, these results suggest that the loss of function of G9a impairs axon formation through a ROCK-dependent effect.

G9a Controls Axonal Growth through a Lfc-Dependent Mechanism

It is now well established that Rho GTPase activity is tightly regulated by GEFs and GTPase activating proteins (GAPs) (Gonzalez-Billault et al., 2012). In neurons, the GEF Lfc, encoded by *Arhgef2*, promotes RhoA activity and ROCK signaling during polarization (Conde et al., 2010). Suppression of Lfc enhances axon formation, while its overexpression inhibits axon outgrowth (Conde et al., 2010). Thus, it became of interest to test whether G9a might regulate Lfc expression during axon formation.

Therefore, we analyzed *Arhgef2* expression in cultured neurons. This analysis revealed a peak of expression 6 h after plating, followed by a significant decrease at 3 DIV (Figure 4A). In contrast, G9a expression peaks 12 h after plating, remaining high thereafter (Figures 1C and 4B), which negatively correlates with *Arhgef2* expression within this time frame (R^2 = 0.911; Figure 4C). By contrast, mRNA levels of RhoA, ROCK, and ARHGEF11 (a RhoA GEF encoded by *Arhgef11*; Mizuki et al., 2016) did not change within the first 72 h of culture (Figures 4D–4F). Moreover, Bix-01294-treated neurons showed an increase in *Arhgef2* expression at 12 h (Figure 4G), suggesting a repressive role for G9a.

G9a lacks DNA binding domains and requires the interaction with proteins to catalyze histone methylation. In this regard, the repressor factor REST recruits G9a through its C-terminal domain (Tachibana et al., 2002; Roopra et al., 2004; Estève et al., 2005) and binds to DNA by recognizing the consensus site "RE1" (regulatory elements 1) (Schoenherr et al., 1996; Bruce et al., 2004; Liu et al., 2009). After an *in silico* analysis, we found several RE1 sites neighboring the transcription start site (TSS) of *Arhgef2*, which prompted us to analyze H3K9me2 levels at the promoter region. Using cultured neurons for 12 h and chromatin immunoprecipitation (ChIP)-qPCR, we detected the H3K9me2 mark at −800 pair base (pb) of the TSS, which was significantly reduced after G9a inhibition (Figure 4H). Moreover, the knockdown of G9a increased Lfc levels in neurons, showing an axonal enrichment (Figures 4I–4M). Finally, expression of shRNA-Lfc-HcRed (Conde et al., 2010) partially rescued axon formation in G9a-suppressed neurons (Figures 4N–4Q). In summary, these data support the notion that G9a inhibits Lfc expression at the time of polarization and axon formation.

DISCUSSION

It is now accepted that positive regulators, acting on a selected neurite, neutralize inhibitory elements, leading to axon specification and growth (Takano et al., 2019). Current evidence favors the view that Lfc-RhoA-ROCK signaling is a major negative factor preventing axon formation (Conde et al., 2010; Takano et al., 2017). Recently, the SMAD-specific E3 ubiquitin protein ligase 1 (SMURF 1) that leads to proteasome degradation of RhoA (Vohra et al., 2007), and Tctex-1 (Chuang et al., 2005), a dynein light chain that binds and inactivates Lfc (Conde et al., 2010), have emerged as factors driving axon outgrowth by counteracting the inhibitory actions of RhoA. We now report on a new

CellPress
OPEN ACCESS

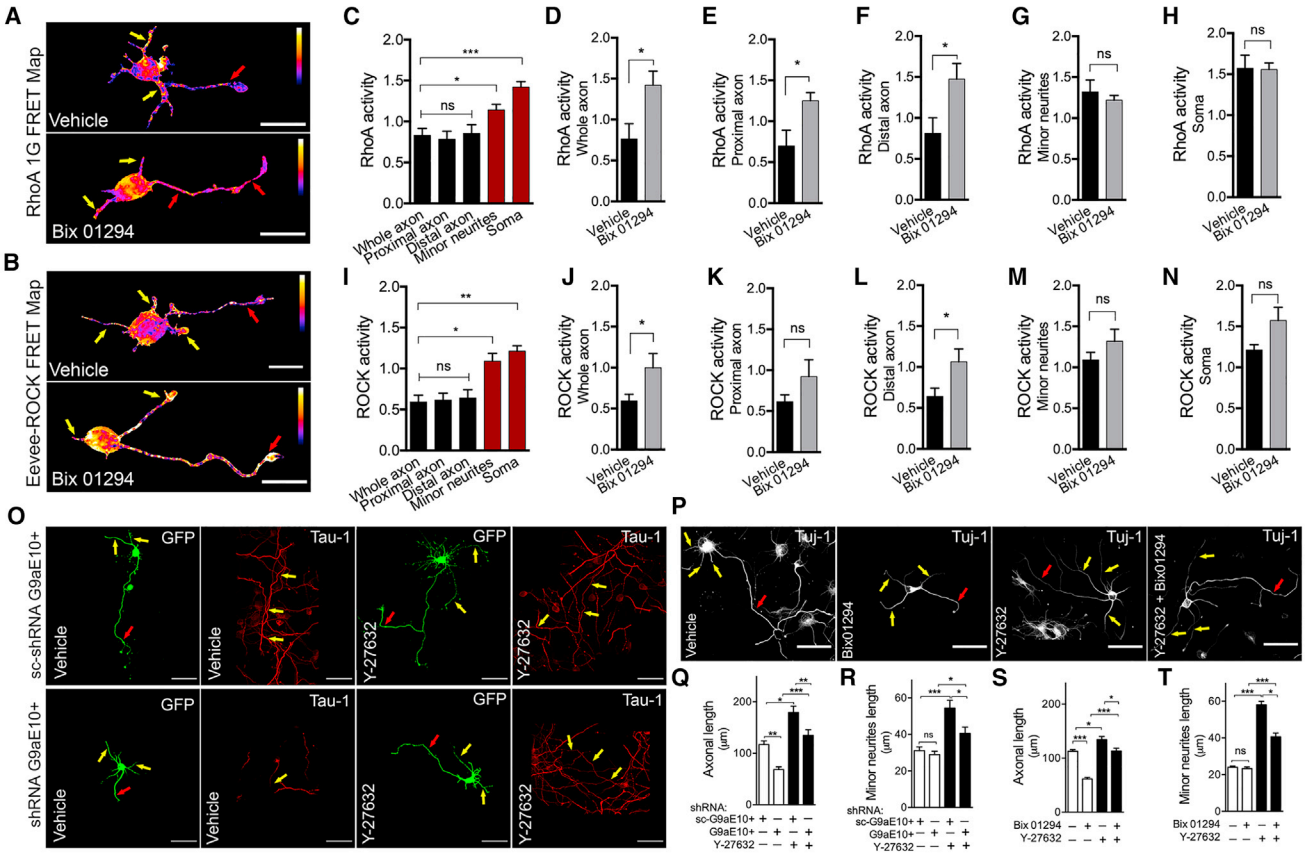

Figure 3. G9a Targets the RhoA Pathway

(A) Images show representative RhoA-1G FRET maps of control and 1 μM Bix-01294-treated neurons. Neurons were transfected after plating with the biosensors and treated with Bix 01294; they were fixed 18 h later.

(B) Images show representative Eevee-ROCK FRET maps of control and 1 μM Bix-01294-treated neurons (transfection, plating and fixation as in A).

(C–N) (C) Quantification of RhoA activity in control neurons. (D) RhoA activity in the whole axon, (E) proximal axon, (F) distal axon, (G) minor neurites and (H) soma in control and Bix-01294-treated neurons. (I) Quantification of ROCK activity in control neurons. (J) ROCK activity in the whole axon, (K) proximal axon, (L) distal axon, (M) minor neurites and (N) soma in control and Bix-01294-treated neurons.

(O) Images showing control or shRNA-G9a/E10+/GFP-expressing neurons. Cells were transfected at the time of plating, treated with Y-27632 (10 μM) 18 h later, and fixed at 2 DIV. Tau-1 IF shows axons (red arrows).

(P) Representative neurons treated with 1 μM Bix 01294 (after plating) and Y-27632 (10 μM) 18 h later, fixed at 2 DIV and stained for Tuj-1 IF.

(Q–T) (Q) Quantification of average axonal length and (R) minor neurites length in control and G9a-suppressed neurons after Y-27632 treatment. (S) Axonal length and (T) minor neurites length in control and 1 μM Bix-01294-treated neurons after 10 μM Y-27632 administration.

Graphs represent mean ± SEM. *p < 0.05, **p < 0.01, ***p < 0.001; ns, non-significant. Kruskal-Wallis, multiple comparisons; (B–D) Student's t test. (A–D) Twenty to 30 transfected neurons were analyzed from five independent cultures (n = 5). (E–J) Thirty transfected neurons were analyzed by each condition from three independent cultures (n= 3). Scale bars: (A and H) 20 μm; (O and P) 50 μm.

mechanism controlling the Lfc-RhoA-ROCK inhibitory axis. Our results provide the first set of evidence suggesting that a mechanism involving the histone methyltransferase G9a controls Lfc expression and RhoA/ROCK activities, affecting axon formation and polarization in developing neurons.

Several lines of evidence support this view. First, the expression and nuclear localization of G9a/E10+ in cultured hippocampal neurons highly correlate with the time course of axon formation. Second, Lfc expression, which is high in unpolarized neurons, negatively correlates with G9a/E10+ levels that rise at the time of axon outgrowth. Third, the loss of function of G9a, either using genetic or pharmacologic tools, inhibited neuronal polarization, evidenced by axonal growth arrest and the absence of a proximo-distal Tau-1 gradient. Besides, the multipolar-bipolar transition fails in cortical neurons developing *in situ* and expressing the shRNA-G9a/E10+/GFP. Moreover, inhibition of G9a reduced H3K9me2 levels of *Arhgef2*, increasing Lfc expression and RhoA-ROCK activities in cultured neurons. Finally, a causal relationship between G9a inhibition/knockdown and up-regulation of the RhoA-ROCK signaling pathway, most likely caused by enhanced Lfc expression, is also supported by the fact that Y-27632 or Lfc suppression rescue axonal growth defects.

Developmental functions of G9a have been reported previously. Thus, G9a depletion impairs embryonic stem cells differentiation by affecting developmental and proliferative programs

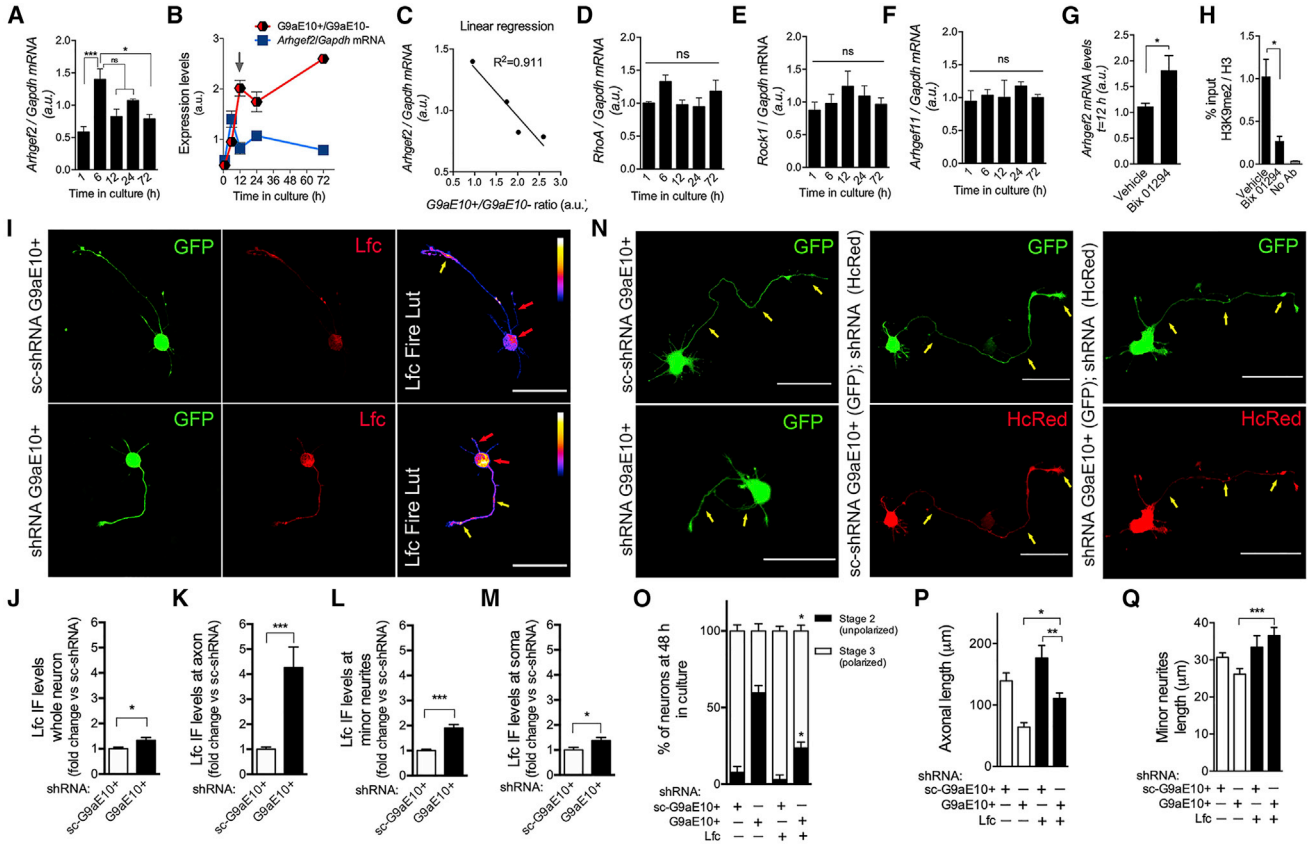

Figure 4. G9a-Dependent Axonal Growth Is Mediated by Lfc Expression

(A) Neurons were cultured for 1–72 h to measure mRNA levels of *Arhgef2* by qRT-PCR.

(B) mRNA levels of *Arhgef2* and G9a/E10+ to G9a/E10− mRNA ratio within the first 3 DIV. Values were obtained from Figure 1C and from (A), respectively, and reproduced here for comparative purposes.

(C) Linear regression plot between *Arhgef2 mRNA* and G9a E10+ /E10− ratio within 6–72 h of culture.

(D) Quantification of *RhoA*, (E) *Rock*, and (F) *Arhgef11 mRNA* as in (A).

(G) *Arhgef2* mRNA levels after 1 μM Bix 01294 treatment (after plating); RNA was isolated 12 h later.

(H) H3K9me2 detection by ChIP-qPCR at −800 pb of TSS of *Arhgef2* in control or Bix-01294-treated cultured neurons (t = 12 h; Bix added after plating).

(I) Representative images showing control and shRNA-G9a/E10+/GFP neurons stained by IF to detect Lfc at 2 DIV.

(J–M) (J) Quantification of Lfc IF levels in whole neuron, (K) axon, (L) minor neurites, and (M) soma.

(N) Images showing representative neurons transfected immediately after plating with sc-shRNA G9aE10+/GFP, shRNA G9aE10+/GFP, sc-shRNA plus shRNA-Lfc-HcRed, and shRNA G9aE10+/GFP plus shRNA-Lfc-HcRed; in all cases, cultures were fixed at 2 DIV.

(O–Q) (O) Quantification of polarity acquisition and (P) axonal and (Q) minor neurites length.

Graphs represent mean ± SEM. *p < 0.05, ***p < 0.001; ns, non-significant. Kruskal-Wallis test, multiple comparisons for (A)–(H), (O), and (P). (D), (E), and (J–N): Student's t test. n = 3 (independent cultures). Scale bar: 50 μm.

(Au Yeung et al., 2019; Feldman et al., 2006; Kim et al., 2016; Liu et al., 2015; Ugarte et al., 2015; Dong et al., 2008). Nevertheless, its contribution to neuronal development is just starting to emerge; in this regard, we previously reported that G9a/E10+ is expressed in N2a cells and required for neurite growth (Fiszbein et al., 2016). In addition, G9a represses the expression of several genes encoding K+ channels after spinal nerve injury, affecting axonal recovery, pain sensitivity, and function (Laumet et al., 2015). Considering this evidence and data presented in our work, we wondered whether G9a could be involved in axonal recovery after injury and neural disorders where the RhoA pathway is dysregulated (Chong et al., 2017). In fact, injured axons improve their growth capacity once ROCK is inhibited (Kubo et al., 2007; Lingor et al., 2007; Planchamp et al., 2008; Rozés Salvador et al., 2016). Thus, chromatin changes controlled by G9a could be important for axonal regrowth after injury.

Our data suggest a selective regulation of Lfc expression, since neither RhoA-ROCK nor GEF11 displays any correlation with G9a/E10+ levels at the time of polarization. However, we cannot rule out that other genes involved in axon formation could also be regulated by G9a. In fact, G9a controls the expression of genes associated with cAMP and Ca^{2+}-dependent signaling (Laumet et al., 2015), which participate in axon formation (Shelly et al., 2010; Muñoz-Llancao et al., 2015; Wilson et al., 2016).

In summary, our work proposes G9a as a player for neuronal polarization, contributing to filling a gap between (epi)genetics and polarity acquisition.

STAR★METHODS

Detailed methods are provided in the online version of this paper and include the following:

- KEY RESOURCES TABLE
- RESOURCE AVAILABILITY
  - Lead Contact
  - Materials Availability
  - Data and Code Availability
- EXPERIMENTAL MODEL AND SUBJECT DETAILS
- METHOD DETAILS
  - Primary culture of hippocampal neurons
  - Cloning of pCAGIG shRNA-G9a/E10+
  - Transient expression of cDNAs by transfection
  - Immunofluorescence and imaging
  - G9a and H3K9me2 nuclear detection
  - Detection of Lfc levels
  - Quantification of polarity, axonal and minor neurites length
  - In utero electroporation (IUE) of E15 embryos and imaging
  - Measurement of RhoA and ROCK activities using FRET biosensors
  - RNA isolation, qRT-PCR analysis and G9a alternative splicing detection
  - H3K9me2 chromatin immunoprecipitation (ChIP)
  - Imaging and post-imaging analysis
- QUANTIFICATION AND STATISTICAL ANALYSIS

SUPPLEMENTAL INFORMATION

Supplemental Information can be found online at https://doi.org/10.1016/j.celrep.2020.107639.

ACKNOWLEDGMENTS

This work was funded by the Consejo Nacional de Investigaciones Científicas y Técnicas (CONICET) and the Agencia Nacional de Promoción Científica y Tecnológica (ANPCYT) of Argentina (grants PICT 2015-1436 and PUE to A.C.; grants PICT-2018-00829 and Lounsbery Foundation (USA) to A.R.K.; grant PICT-2018-01684 to C.W.). A.C., L.E.G., and A.R.K. are investigators, and C.W. and V.R.-S. are postdoctoral fellows of CONICET.

AUTHOR CONTRIBUTIONS

All authors designed experimental procedures. C.W. performed experiments. Alternative splicing assays, ChIP assays, and qPCR detections were done by L.E.G. and C.W. V.R.-S. performed IUE. All authors wrote the paper. A.C. and A.R.K. secured funding.

DECLARATION OF INTERESTS

The authors declare no competing interests.

Received: November 11, 2019
Revised: March 18, 2020
Accepted: April 21, 2020
Published: May 12, 2020

REFERENCES

Amano, M., Kaneko, T., Maeda, A., Nakayama, M., Ito, M., Yamauchi, T., Goto, H., Fukata, Y., Oshiro, N., Shinohara, A., et al. (2003). Identification of Tau and MAP2 as novel substrates of Rho-kinase and myosin phosphatase. J. Neurochem. *87*, 780–790.

Au Yeung, W.K., Brind'Amour, J., Hatano, Y., Yamagata, K., Feil, R., Lorincz, M.C., Tachibana, M., Shinkai, Y., and Sasaki, H. (2019). Histone H3K9 Methyltransferase G9a in Oocytes Is Essential for Preimplantation Development but Dispensable for CG Methylation Protection. Cell Rep. *27*, 282–293.e284.

Barnes, A.P., and Polleux, F. (2009). Establishment of axon-dendrite polarity in developing neurons. Annu. Rev. Neurosci. *32*, 347–381.

Bian, C., Chen, Q., and Yu, X. (2015). The zinc finger proteins ZNF644 and WIZ regulate the G9a/GLP complex for gene repression. eLife *4*.

Binder, L.I., Frankfurter, A., and Rebhun, L.I. (1985). The distribution of tau in the mammalian central nervous system. J. Cell Biol. *101*, 1371–1378.

Bradke, F., and Dotti, C.G. (1997). Neuronal polarity: vectorial cytoplasmic flow precedes axon formation. Neuron *19*, 1175–1186.

Bruce, A.W., Donaldson, I.J., Wood, I.C., Yerbury, S.A., Sadowski, M.I., Chapman, M., Göttgens, B., and Buckley, N.J. (2004). Genome-wide analysis of repressor element 1 silencing transcription factor/neuron-restrictive silencing factor (REST/NRSF) target genes. Proc. Natl. Acad. Sci. USA *101*, 10458–10463.

Cáceres, A., Ye, B., and Dotti, C.G. (2012). Neuronal polarity: demarcation, growth and commitment. Curr. Opin. Cell Biol. *24*, 547–553.

Cánovas, J., Berndt, F.A., Sepúlveda, H., Aguilar, R., Veloso, F.A., Montecino, M., Oliva, C., Maass, J.C., Sierralta, J., and Kukuljan, M. (2015). The Specification of Cortical Subcerebral Projection Neurons Depends on the Direct Repression of TBR1 by CTIP1/BCL11a. J. Neurosci. *35*, 7552–7564.

Chong, C.M., Ai, N., and Lee, S.M. (2017). ROCK in CNS: Different Roles of Isoforms and Therapeutic Target for Neurodegenerative Disorders. Curr. Drug Targets *18*, 455–462.

Chuang, J.Z., Yeh, T.Y., Bollati, F., Conde, C., Canavosio, F., Cáceres, A., and Sung, C.-H. (2005). The dynein light chain Tctex-1 has a dynein-independent role in actin remodeling during neurite outgrowth. Dev. Cell *9*, 75–86.

Conde, C., Arias, C., Robin, M., Li, A., Saito, M., Chuang, J.Z., Nairn, A.C., Sung, C.H., and Cáceres, A. (2010). Evidence for the involvement of Lfc and Tctex-1 in axon formation. J. Neurosci. *30*, 6793–6800.

Darenfed, H., Dayanandan, B., Zhang, T., Hsieh, S.H., Fournier, A.E., and Mandato, C.A. (2007). Molecular characterization of the effects of Y-27632. Cell Motil. Cytoskeleton *64*, 97–109.

Dong, K.B., Maksakova, I.A., Mohn, F., Leung, D., Appanah, R., Lee, S., Yang, H.W., Lam, L.L., Mager, D.L., Schübeler, D., et al. (2008). DNA methylation in ES cells requires the lysine methyltransferase G9a but not its catalytic activity. EMBO J. *27*, 2691–2701.

Dupraz, S., Hilton, B.J., Husch, A., Santos, T.E., Coles, C.H., Stern, S., Brakebusch, C., and Bradke, F. (2019). RhoA Controls Axon Extension Independent of Specification in the Developing Brain. Curr. Biol. *29*, 3874–3886.e9.

Estève, P.O., Patnaik, D., Chin, H.G., Benner, J., Teitell, M.A., and Pradhan, S. (2005). Functional analysis of the N- and C-terminus of mammalian G9a histone H3 methyltransferase. Nucleic Acids Res. *33*, 3211–3223.

Feldman, N., Gerson, A., Fang, J., Li, E., Zhang, Y., Shinkai, Y., Cedar, H., and Bergman, Y. (2006). G9a-mediated irreversible epigenetic inactivation of Oct-3/4 during early embryogenesis. Nat. Cell Biol. *8*, 188–194.

Fiszbein, A., and Kornblihtt, A.R. (2016). Histone methylation, alternative splicing and neuronal differentiation. Neurogenesis (Austin) *3*, e1204844.

Fiszbein, A., Giono, L.E., Quaglino, A., Berardino, B.G., Sigaut, L., von Bilderling, C., Schor, I.E., Steinberg, J.H., Rossi, M., Pietrasanta, L.I., et al. (2016). Alternative Splicing of G9a Regulates Neuronal Differentiation. Cell Rep. *14*, 2797–2808.

Fritz, R.D., Letzelter, M., Reimann, A., Martin, K., Fusco, L., Ritsma, L., Ponsioen, B., Fluri, E., Schulte-Merker, S., van Rheenen, J., and Pertz, O.

(2013). A versatile toolkit to produce sensitive FRET biosensors to visualize signaling in time and space. Sci. Signal. *6*, rs12.

Fuentes, P., Cánovas, J., Berndt, F.A., Noctor, S.C., and Kukuljan, M. (2012). CoREST/LSD1 control the development of pyramidal cortical neurons. Cereb. Cortex *22*, 1431–1441.

Gardner, K.E., Allis, C.D., and Strahl, B.D. (2011). Operating on chromatin, a colorful language where context matters. J. Mol. Biol. *409*, 36–46.

Gonzalez-Billault, C., Muñoz-Llancao, P., Henriquez, D.R., Wojnacki, J., Conde, C., and Caceres, A. (2012). The role of small GTPases in neuronal morphogenesis and polarity. Cytoskeleton (Hoboken) *69*, 464–485.

Hatanaka, Y., and Yamauchi, K. (2013). Excitatory cortical neurons with multipolar shape establish neuronal polarity by forming a tangentially oriented axon in the intermediate zone. Cereb. Cortex *23*, 105–113.

Hwang, J.Y., Aromolaran, K.A., and Zukin, R.S. (2017). The emerging field of epigenetics in neurodegeneration and neuroprotection. Nat. Rev. Neurosci. *18*, 347–361.

Kaech, S., and Banker, G. (2006). Culturing hippocampal neurons. Nat. Protoc. *1*, 2406–2415.

Kim, H.T., Jeong, S.G., and Cho, G.W. (2016). G9a inhibition promotes neuronal differentiation of human bone marrow mesenchymal stem cells through the transcriptional induction of RE-1 containing neuronal specific genes. Neurochem. Int. *96*, 77–83.

Kriegstein, A.R., and Noctor, S.C. (2004). Patterns of neuronal migration in the embryonic cortex. Trends Neurosci. *27*, 392–399.

Kubicek, S., O'Sullivan, R.J., August, E.M., Hickey, E.R., Zhang, Q., Teodoro, M.L., Rea, S., Mechtler, K., Kowalski, J.A., Homon, C.A., et al. (2007). Reversal of H3K9me2 by a small-molecule inhibitor for the G9a histone methyltransferase. Mol. Cell *25*, 473–481.

Kubo, T., Hata, K., Yamaguchi, A., and Yamashita, T. (2007). Rho-ROCK inhibitors as emerging strategies to promote nerve regeneration. Curr. Pharm. Des. *13*, 2493–2499.

Laumet, G., Garriga, J., Chen, S.R., Zhang, Y., Li, D.P., Smith, T.M., Dong, Y., Jelinek, J., Cesaroni, M., Issa, J.P., and Pan, H.L. (2015). G9a is essential for epigenetic silencing of K(+) channel genes in acute-to-chronic pain transition. Nat. Neurosci. *18*, 1746–1755.

Li, C., Imanishi, A., Komatsu, N., Terai, K., Amano, M., Kaibuchi, K., and Matsuda, M. (2017). A FRET Biosensor for ROCK Based on a Consensus Substrate Sequence Identified by KISS Technology. Cell Struct. Funct. *42*, 1–13.

Liang, L., Gu, X., Zhao, J.Y., Wu, S., Miao, X., Xiao, J., Mo, K., Zhang, J., Lutz, B.M., Bekker, A., and Tao, Y.X. (2016a). G9a participates in nerve injury-induced Kcna2 downregulation in primary sensory neurons. Sci. Rep. *6*, 37704.

Liang, L., Zhao, J.Y., Gu, X., Wu, S., Mo, K., Xiong, M., Marie Lutz, B., Bekker, A., and Tao, Y.X. (2016b). G9a inhibits CREB-triggered expression of mu opioid receptor in primary sensory neurons following peripheral nerve injury. Mol. Pain *12*, 1744806916682242.

Lingor, P., Teusch, N., Schwarz, K., Mueller, R., Mack, H., Bähr, M., and Mueller, B.K. (2007). Inhibition of Rho kinase (ROCK) increases neurite outgrowth on chondroitin sulphate proteoglycan in vitro and axonal regeneration in the adult optic nerve in vivo. J. Neurochem. *103*, 181–189.

Liu, Z., Liu, M., Niu, G., Cheng, Y., and Fei, J. (2009). Genome-wide identification of target genes repressed by the zinc finger transcription factor REST/NRSF in the HEK 293 cell line. Acta Biochim. Biophys. Sin. (Shanghai) *41*, 1008–1017.

Liu, N., Zhang, Z., Wu, H., Jiang, Y., Meng, L., Xiong, J., Zhao, Z., Zhou, X., Li, J., Li, H., et al. (2015). Recognition of H3K9 methylation by GLP is required for efficient establishment of H3K9 methylation, rapid target gene repression, and mouse viability. Genes Dev. *29*, 379–393.

Mandell, J.W., and Banker, G.A. (1996). A spatial gradient of tau protein phosphorylation in nascent axons. J. Neurosci. *16*, 5727–5740.

Mizuki, Y., Takaki, M., Sakamoto, S., Okamoto, S., Kishimoto, M., Okahisa, Y., Itoh, M., and Yamada, N. (2016). Human Rho Guanine Nucleotide Exchange Factor 11 (ARHGEF11) Regulates Dendritic Morphogenesis. Int. J. Mol. Sci. *18*, E67.

Mozzetta, C., Pontis, J., Fritsch, L., Robin, P., Portoso, M., Proux, C., Margueron, R., and Ait-Si-Ali, S. (2014). The histone H3 lysine 9 methyltransferases G9a and GLP regulate polycomb repressive complex 2-mediated gene silencing. Mol. Cell *53*, 277–289.

Muñoz-Llancao, P., Henríquez, D.R., Wilson, C., Bodaleo, F., Boddeke, E.W., Lezoualc'h, F., Schmidt, M., and González-Billault, C. (2015). Exchange Protein Directly Activated by cAMP (EPAC) Regulates Neuronal Polarization through Rap1B. J. Neurosci. *35*, 11315–11329.

Nakamuta, S., Funahashi, Y., Namba, T., Arimura, N., Picciotto, M.R., Tokumitsu, H., Soderling, T.R., Sakakibara, A., Miyata, T., Kamiguchi, H., and Kaibuchi, K. (2011). Local application of neurotrophins specifies axons through inositol 1,4,5-trisphosphate, calcium, and Ca2+/calmodulin-dependent protein kinases. Sci. Signal. *4*, ra76.

Namba, T., Funahashi, Y., Nakamuta, S., Xu, C., Takano, T., and Kaibuchi, K. (2015). Extracellular and Intracellular Signaling for Neuronal Polarity. Physiol. Rev. *95*, 995–1024.

Olsen, J.B., Wong, L., Deimling, S., Miles, A., Guo, H., Li, Y., Zhang, Z., Greenblatt, J.F., Emili, A., and Tropepe, V. (2016). G9a and ZNF644 Physically Associate to Suppress Progenitor Gene Expression during Neurogenesis. Stem Cell Reports *7*, 454–470.

Palomer, E., Carretero, J., Benvegnù, S., Dotti, C.G., and Martin, M.G. (2016). Neuronal activity controls Bdnf expression via Polycomb de-repression and CREB/CBP/JMJD3 activation in mature neurons. Nat. Commun. *7*, 11081.

Planchamp, V., Bermel, C., Tönges, L., Ostendorf, T., Kügler, S., Reed, J.C., Kermer, P., Bähr, M., and Lingor, P. (2008). BAG1 promotes axonal outgrowth and regeneration in vivo via Raf-1 and reduction of ROCK activity. Brain *131*, 2606–2619.

Quassollo, G., Wojnacki, J., Salas, D.A., Gastaldi, L., Marzolo, M.P., Conde, C., Bisbal, M., Couve, A., and Cáceres, A. (2015). A RhoA Signaling Pathway Regulates Dendritic Golgi Outpost Formation. Curr. Biol. *25*, 971–982.

Roopra, A., Qazi, R., Schoenike, B., Daley, T.J., and Morrison, J.F. (2004). Localized domains of G9a-mediated histone methylation are required for silencing of neuronal genes. Mol. Cell *14*, 727–738.

Rozés Salvador, V., Heredia, F., Berardo, A., Palandri, A., Wojnacki, J., Vivinetto, A.L., Sheikh, K.A., Caceres, A., and Lopez, P.H. (2016). Anti-glycan antibodies halt axon regeneration in a model of Guillain Barrè Syndrome axonal neuropathy by inducing microtubule disorganization via RhoA-ROCK-dependent inactivation of CRMP-2. Exp. Neurol. *278*, 42–53.

Schoenherr, C.J., Paquette, A.J., and Anderson, D.J. (1996). Identification of potential target genes for the neuron-restrictive silencer factor. Proc. Natl. Acad. Sci. USA *93*, 9881–9886.

Sharma, M., and Sajikumar, S. (2019). G9a/GLP Complex Acts as a Bidirectional Switch to Regulate Metabotropic Glutamate Receptor-Dependent Plasticity in Hippocampal CA1 Pyramidal Neurons. Cereb. Cortex *29*, 2932–2946.

Sharma, M., Dierkes, T., and Sajikumar, S. (2017a). Epigenetic regulation by G9a/GLP complex ameliorates amyloid-beta 1-42 induced deficits in long-term plasticity and synaptic tagging/capture in hippocampal pyramidal neurons. Aging Cell *16*, 1062–1072.

Sharma, M., Razali, N.B., and Sajikumar, S. (2017b). Inhibition of G9a/GLP Complex Promotes Long-Term Potentiation and Synaptic Tagging/Capture in Hippocampal CA1 Pyramidal Neurons. Cereb. Cortex *27*, 3161–3171.

Shelly, M., Lim, B.K., Cancedda, L., Heilshorn, S.C., Gao, H., and Poo, M.M. (2010). Local and long-range reciprocal regulation of cAMP and cGMP in axon/dendrite formation. Science *327*, 547–552.

Shinkai, Y., and Tachibana, M. (2011). H3K9 methyltransferase G9a and the related molecule GLP. Genes Dev. *25*, 781–788.

Stiess, M., and Bradke, F. (2011). Neuronal polarization: the cytoskeleton leads the way. Dev. Neurobiol. *71*, 430–444.

Tachibana, M., Sugimoto, K., Nozaki, M., Ueda, J., Ohta, T., Ohki, M., Fukuda, M., Takeda, N., Niida, H., Kato, H., and Shinkai, Y. (2002). G9a histone

methyltransferase plays a dominant role in euchromatic histone H3 lysine 9 methylation and is essential for early embryogenesis. Genes Dev. *16*, 1779–1791.

Tachibana, M., Matsumura, Y., Fukuda, M., Kimura, H., and Shinkai, Y. (2008). G9a/GLP complexes independently mediate H3K9 and DNA methylation to silence transcription. EMBO J. *27*, 2681–2690.

Takano, T., Wu, M., Nakamuta, S., Naoki, H., Ishizawa, N., Namba, T., Watanabe, T., Xu, C., Hamaguchi, T., Yura, Y., et al. (2017). Discovery of long-range inhibitory signaling to ensure single axon formation. Nat. Commun. *8*, 33.

Takano, T., Funahashi, Y., and Kaibuchi, K. (2019). Neuronal Polarity: Positive and Negative Feedback Signals. Front. Cell Dev. Biol. *7*, 69.

Tan, M., Luo, H., Lee, S., Jin, F., Yang, J.S., Montellier, E., Buchou, T., Cheng, Z., Rousseaux, S., Rajagopal, N., et al. (2011). Identification of 67 histone marks and histone lysine crotonylation as a new type of histone modification. Cell *146*, 1016–1028.

Ugarte, F., Sousae, R., Cinquin, B., Martin, E.W., Krietsch, J., Sanchez, G., Inman, M., Tsang, H., Warr, M., Passegué, E., et al. (2015). Progressive Chromatin Condensation and H3K9 Methylation Regulate the Differentiation of Embryonic and Hematopoietic Stem Cells. Stem Cell Reports *5*, 728–740.

Vohra, B.P., Fu, M., and Heuckeroth, R.O. (2007). Protein kinase Czeta and glycogen synthase kinase-3beta control neuronal polarity in developing rodent enteric neurons, whereas SMAD specific E3 ubiquitin protein ligase 1 promotes neurite growth but does not influence polarity. J. Neurosci. *27*, 9458–9468.

Wilson, C., Muñoz-Palma, E., Henríquez, D.R., Palmisano, I., Núñez, M.T., Di Giovanni, S., and González-Billault, C. (2016). A Feed-Forward Mechanism Involving the NOX Complex and RyR-Mediated Ca2+ Release During Axonal Specification. J. Neurosci. *36*, 11107–11119.

Xu, C., Funahashi, Y., Watanabe, T., Takano, T., Nakamuta, S., Namba, T., and Kaibuchi, K. (2015). Radial Glial Cell-Neuron Interaction Directs Axon Formation at the Opposite Side of the Neuron from the Contact Site. J. Neurosci. *35*, 14517–14532.

STAR★METHODS

KEY RESOURCES TABLE

REAGENT or RESOURCE	SOURCE	IDENTIFIER
Antibodies		
Anti-tubulin class III	Abcam	ab78078; RRID:AB_2256751
Anti-Ehmt2 antibody (G9a)	Sigma	SAB2700645
Anti-Tau1	Lester Binder's laboratory (Binder et al., 1985)	N/A
Anti-Tau5	Lester Binder's laboratory (Binder et al., 1985)	N/A
Anti-Lfc	Dianova	X1089P
Anti-H3K9me2	Abcam	ab1220; RRID:AB_449854
Anti-H3	Millipore	07-690; RRID:AB_417398
Alexa Fluor 546 anti-sheep	LifeTechnologies	A21098; RRID:AB_1500708
Alexa Fluor 488 anti-mouse	LifeTechnologies	A11029; RRID:AB_138404
Alexa Fluor 568 anti-mouse	LifeTechnologies	A11004; RRID:AB_2534072
Alexa Fluor 546 anti-rabbit	LifeTechnologies	A11010; RRID:AB_2534077
Chemicals, Peptides, and Recombinant Proteins		
Bix 01294 trihydrochloride hydrate	SIGMA	B9311
Y-27632 dyhidrochloride	Merck Millipore	688000
Experimental Models: Organisms/Strains		
Rat: Wistar	Produced in the animal facility of Instituto de Investigación Médica Mercedes y Martin Ferreyra (Córdoba, Argentina); originally from Charles River, USA.	N/A
Mouse: C57BL/6N	Produced in the animal facility of Instituto de Investigación Médica Mercedes y Martin Ferreyra (Córdoba, Argentina); originally from Universidad Nacional de la Plata (La Plata, Argentina).	N/A
Oligonucleotides		
	See Table S1 for primers and oligonucleotides used in this paper.	N/A
Recombinant DNA		
pCAGIG shRNA-G9a/E10+ (shRNA G9aE10+/GFP)	This paper	N/A
pCAGIG sc-shRNA-G9a/E10+ (sc-shRNA G9aE10+(GFP)	This paper	N/A
RhoA 1G FRET biosensor	Fritz et al., 2013	N/A
Eevee ROCK FRET biosensor	Li et al., 2017	N/A
pCAG-HcRed shRNA-Lfc	Conde et al., 2010	N/A

RESOURCE AVAILABILITY

Lead Contact

Further information and requests for resources/reagents should be directed to and will be fulfilled by the Lead Contact, Alfredo Cáceres (acaceres@immf.uncor.edu).

Materials Availability

The plasmid pCAGIG shRNA-G9a/E10+/GFP was generated in this study. For further information and request, please contact Dr. Alfredo Cáceres.

Data and Code Availability

This study did not generate/analyze datasets.

EXPERIMENTAL MODEL AND SUBJECT DETAILS

Wild-type E18.5 pregnant wistar rats and wild-type E15.5 pregnant C57BL/6N mice were produced and housed at the animal facility of Instituto de Investigación Médica Mercedes y Martin Ferreyra (INIMEC-CONICET-UNC), following Institutional Animal Care and Use Committee (CICUAL) and NIH guidelines. All procedures were approved by the CICUAL of INIMEC. Male and female animals were matched in this study.

METHOD DETAILS

Primary culture of hippocampal neurons

Hippocampal neuronal cultures were prepared according to Kaech and Banker, 2006 (see also Conde et al., 2010). Briefly, either hippocampus or cortices were isolated from embryonic rat brain of E18.5 days, followed by enzymatic and mechanical dissociation. Neurons were seeded on either plastic culture dishes or glass coverslips, both pre-treated with poly-L-lysine (PLL) (1 mg/ml) overnight. For plating, neurons were cultured for 1 h in Dulbecco's Modified Eagle's Medium (DMEM) supplemented with 10% horse serum. Then, plating medium was replaced by Neurobasal culture medium supplemented with B27 Plus, Glutamax and antibiotics (penicillin and streptomycin). For transfection and non-transfection assays, $5x10^4$ and $2x10^4$ cells/coverslip were plated, respectively. Animal procedures followed the guidelines of NIH and institutional animal care and use committee of Instituto Ferreyra.

Cloning of pCAGIG shRNA-G9a/E10+

Briefly, we chose a sequence contained in the exon 10 to specifically knock-down this splicing variant. Of note, exon 10 sequence is conserved in rat and mouse. Target sequence was 5′ GGGGTCCCTGGAGCTGCCCAG 3′. Following the protocol, we ordered 4 oligonucleotides (Macrogen) to clone the shRNA coding sequence cassette into the pB6/U6 plasmid (1a: GGGTCCCTGGAGCTGCCCAGA, 1b: AGCTTCTGGGCAGCTCCAGGGACCC, 2a: AGCTTCTGGGCAGCTCCAGGGACCCCT TTTTG, 2b: AATTCAAAAAGGGGTCCCTGGAGCTGCCCAGA). Then, cloning into pB6/U6 plasmid was done in two steps (for each pair of oligonucleotides). For annealing, oligonucleotides 1a and 1b were dissolved in buffer NEB 3 (New England BioLabs) heated at 100°C for 5 min and then chill up to reach RT (2h). Then, annealed oligonucleotides 1a+1b were cloned into the pB6/U6 plasmid, previously digested with ApaI, treated with Klenow to blunt 3′protruding end and finally digested with HindIII (A/K/H). Thus, annealed 1a+1b oligonucleotides were ligated into a purified pB6/U6 (A/K/H) using a DNA ligase T4 for 1 h at RT (pB6/U6 ^{1st}). Then, pB6/U6 1^{st} was purified for the 2^{nd} step of cloning. Accordingly, pB6/U6 1^{st} was digested with EcoRI and HindIII and then purified using a GenJet Gel Extraction kit (ThermoFisher Scientific). Annealed oligonucleotides 2a and 2b were then ligated into pB6/U6 (pB6/U6 2^{nd}). Then, pB6/U6 2^{nd} was amplified in DH5α cells and colonies (Amp-resistant) were selected for DNA purification using a GenJet miniprep kit (ThermoFisher). Purified pB6/U6 2^{nd} was sequenced in Macrogen (Korea) to check proper shRNA reconstruction. Then, U6-shRNA-containing cassette was digested from pB6/U6 2^{nd} and subcloned into a GFP-expressing plasmid under CAG U6 promoter (pCAGIG). For this, pB6/U6 2^{nd} was digested with SpeI, purified and then ligated into a SpeI-digested pCAGIG plasmid. Then, ligation product was purified from gel and amplified in DH5α cells overnight. Amp-resistant bacteria were selected for DNA purification (GenJet midiprep kit, ThermoFisher).

Transient expression of cDNAs by transfection

After 1 h of plating in MEM supplemented with 10% HS, neurons were transfected with Lipofectamine 2000. For this, plating medium was replaced by Neurobasal medium without any supplement. Both DNA and Lipofectamine were mixed in Optimem medium and then added to neurons in Neurobasal, following manufacturer's instructions. After 2 h of transfection was stopped by replacing medium by Neurobasal supplemented with B27, Glutamax and antibiotics for the time of each experiment. All these reagents were purchased from Thermo Fisher Scientific – Lifetechnologies (USA).

Immunofluorescence and imaging

Neurons were fixed with a solution containing 4% w/v paraformaldehyde and 4% sucrose (SIGMA), diluted in phosphate buffered saline (PBS) solution for 20 min at RT. Fixed cultures were then washed 3 times with PBS followed by permeabilization with 0.2% Triton X-100 in PBS for 5 min at RT. For immunofluorescence, permeabilized cells were incubated for 2 h with primary antibodies diluted accordingly in 0.1% v/v Tween-PBS solution. Three 10 -min washes with PBS were done before incubation with secondary antibody incubation. For this, secondary antibodies conjugated with fluorochromes (AlexaFluor488 nm, 568 nm and 633 nm from ThermoFisher) were diluted (1: 1,000) in 0.1% v/v Tween-PBS solution for 1 h at RT in a dark-wet chamber. Then, cells were washed 3 times with PBS and mounted with Mowiol (SIGMA) reagent on glass slides. Samples were stored at 4°C until imaging. Z stack imaging was done in an LSM 800 microscopy (Zeiss, Germany) using a 40x oil objective and 1 airy unit (a.u.). Reconstruction and post-imaging analysis were done in Fiji-ImageJ (NIH, USA). Antibodies used in this study: mouse monoclonal antibody (mAb) Tau-1 (diluted, 1:400) Tuj-1 (mAb against the neuron-specific class III β-tubulin, 1:1,000, Abcam, #ab78078); Tau-5 (a mAb that recognizes a dephosphorylated epitope and thus served to detect total Tau protein, 1:400). Tau-1 and Tau-5 mAbs were a generous gift from Dr. Lester I. Binder (Binder et al., 1985).

G9a and H3K9me2 nuclear detection

G9a or H3K9me2 mark was detected in cultured neurons following the protocol of immunofluorescence described. Fixed neurons were stained with anti-G9a (Anti-Ehmt2, 1:1000, rabbit, SIGMA, #SAB2700645) for 1 h at RT or anti-H3K9me2 antibody (Abcam, 1:300, mouse, #1220) overnight at 4°C, followed by secondary antibody incubation (anti-rabbit AlexaFluor 568 nm or anti-mouse AlexaFluor 568, ThermoFisher) for 1 h. After washing, a final incubation of 5 min with DAPI (1: 10,000) was done for nuclear staining. Image acquisition was achieved by z stack imaging for either G9a or H3K9me2 and DAPI fluorescence using a Zeiss LSM 800 confocal microscopy. In order to quantify G9a and H3K9me2 nuclear levels, total G9a fluorescence and DAPI staining were calculated throughout z axis using the "z-project/sum slices" plug-in of Fiji-ImageJ. Then, a nuclear ROI was measure, defined by DAPI fluorescence projection. G9a and H3K9me2 nuclear fluorescences were divided by DAPI staining to normalize the nuclear volume of each cell.

Detection of Lfc levels

Lfc was detected in neurons transfected after plating with sc-shRNA-G9a/E10+/GFP or shRNA-G9a/E10+/GFP and fixed at 2 DIV, following the protocol of immunofluorescence described. Fixed neurons were stained with an antibody anti-Lfc (Dianova, #X1089P, lot no: 9138, sheep, 1:250) overnight (16-18 h) at 4°C followed by secondary antibody incubation (anti-sheep AlexaFluor 546 nm, ThermoFisher) for 1 h at RT. Image acquisition was achieved by z stack imaging using a Zeiss LSM 800 confocal microscopy. In order to quantify Lfc levels, total Lfc fluorescence was calculated throughout z axis using the "z-project/sum slices" plug-in of Fiji-ImageJ. Then, a line was drawn throughout the axon and minor neurites, or a ROI for somatic IF signal, to measure mean fluorescence levels in each compartment.

Quantification of polarity, axonal and minor neurites length

Neurons displaying a symmetric array of neurites of 20-40 μm in length were considered to be at stage 2. By contrast, neurons exhibiting a single neurite of at least 100 μm (or more), or 2-3 times longer than any one of the other minor processes of the same cell, were considered to be at stage 3. Neurite lengths (axonal and minor neurites) were quantified using the segmented line tool of Fiji-ImageJ.

In utero electroporation (IUE) of E15 embryos and imaging

IUE were done following previous reports (Cánovas et al., 2015; Fuentes et al., 2012). Briefly, pregnant E15 C57BL/6 mice were anesthetized with isofluorane (4% for induction and 2% for maintenance) during the whole surgery, using Tramadol (5 mg/kg) as analgesia during the procedure. Embryos were exposed out of the maternal belly for local injection of cDNA-encoding plasmids into lateral ventricle of the brain. To visualize successful injections, the fast green FCF dye (Sigma-Aldrich, #F7252) was co-injected with DNAs. Then, brains were electroporated using a BTX electroporator with Tweezers w/Variable Gap 2 Square Platinum Electrodes (Nepagene, CUY647P2X2) (ΔV = 39 V; pulses: 5; duration: 50 ms; intervals between pulses: 950 ms). After electroporation, in utero embryos were returned to the maternal belly to follow with the recovery of the mother. Two days after surgery (E17.5), they were sacrificed to check for GFP expression in both control and shRNA-G9a/E10+ genetic contexts. Brains expressing GFP were fixed in 4% w/v paraformaldehyde solution dissolved in PBS overnight at 4°C with gentle agitation. Then, fixed brains were immersed into a 30% w/v sucrose solution for 24 h at 4°C. Post-fixed brains were frozen at −20°C using Crioplast solution (Biopack). Cerebral cortex was sliced into 40 μm cortical sections using a cryostat (Leica CM 1850). Brain slices were mounted into glass slides. Tissues were permeabilized with 0.3% v/v Triton X-100-PBS solution, followed by DAPI staining (15 min at RT). Then, samples were mounted in Mowiol solution (Sigma) for z stack imaging in a Zeiss LSM-800 confocal microscopy. Images were acquired with a 20x oil objective. Several fields were acquired by slice in order to reconstruct the whole tissue (from the ventricular zone to the cortical plate). Thus, images were then stitched using the Stitching plug-in of Fiji-ImageJ. Images shown in Figure 2 represent the maximal intensity of fluorescence, generated with the z-project/maximal intensity plug-in of Fiji-ImageJ. Animal procedures followed the guidelines of NIH and institutional animal care and use committee of Instituto Ferreyra.

Measurement of RhoA and ROCK activities using FRET biosensors

Neurons were culture for 18 h on 24-multiwell containing glass coverslips (12 mm diameter, $5x10^4$ neurons/coverslip) pre-treated with PLL overnight. Neurons were transfected 1 h after plating with plasmids encoding FRET-based biosensors to measure either RhoA or ROCK activity (Fritz et al., 2013; Quassollo et al., 2015; Li et al., 2017). Transfection was done following our transient transfection method, using 400 ng per well. In order to avoid overexpression, neurons were fixed with a 4% w/v paraformaldehyde/sucrose solution at 18 h of culture. To estimate FRET efficiency, an Olympus IX81inverted microscope equipped with a DSU device, fluorescence illumination (100 W mercury arc lamp), and a microprocessor were used. CFP (donor channel) was excited with a 433 nm laser and emission was collected 475 nm. Acceptor channel (FRET) was excited with a 433 nm laser and emission was collected at 527 nm. FRET map was obtained by the dividing the processed image of the FRET channel over the image of the donor channel. To exclude from the analysis out-of-cell pixels, a 0-1 intensity binary mask was created using FRET channel images and multiplied by the FRET map images. FRET maps and their quantifications were done using Fiji-ImageJ (NIH, USA), by drawing a line in neurites (axon or minor neurites) or by defining a somatic ROI (for somas). The values shown represent mean FRET efficiency in each neuronal compartment.

RNA isolation, qRT-PCR analysis and G9a alternative splicing detection

Neurons were cultured on 35 mm plastic dishes pre-treated with PLL overnight (10^6 cells/dish). Control and Bix-01294-treated neurons were cultured for 1 DIV. Bix-01294 (or vehicle) was added to the culture medium 1 h after plating and maintained up to the moment of RNA isolation. For this, neurons were lysed and resuspended in Trizol reagent (Lifetechnologies) following the manufacturer's instructions. cDNA was then generated by reverse transcriptase using Superscript IV RT (ThermoFisher) or M-MLV RT (Promega), following datasheet guidelines. Quantitative PCR reactions were done using a StepOne Real Time PCR system (Applied Biosystems) with SYBR Green master mix (Life Technologies) with the following primers: Rat *Arhgef2* Fw: AGCATTACAGCCAAG GAAGC, Rv: AGCAGTGCAGCTTTCTGTTG; Rat *Gapdh* Fw: AACTTTGGCATCGTGGAAGG, Rv: TGGATGCAGGGATGATGTTCTG. Rat *ROCK1* Fw: AGGGACATCATGGCATTTGC, Rv: TTCAGGCACATCGTAGTTGC; Rat *RhoA* Fw: TTATGTGCCCACGGTGTTTG, Rv: TGTCCAGCTGTGTCCCATAAAG. To detect G9a/E10+ and G9a/E10- splicing variants in cultured hippocampal neurons, RNA was isolated from cultured cells at different times of culture to detect alternative splicing by radioactive PCR, using a Bio-Rad T100 cycler with the following primers: Fw: GGGTGAAGCCATCCAGGAAA, Rv: CTCTCCGTCCACACTTTCGG. A ratio between G9a/E10+ and G9a/E10- variants was established as a measurement of G9a/E10+ enrichment during neuronal polarization.

H3K9me2 chromatin immunoprecipitation (ChIP)

For ChIP assays, cortical neurons were isolated from E18.5 brain rat embryos and cultured into 10 mm plastic dishes ($1.5x10^7$ neurons/dish). Neurons were treated immediately after plating with 1 μM Bix-01294 or vehicle (water) for 12 h. Then, chromatin was isolated for ChIP reactions following the protocol described in Palomer et al., 2016. Briefly, neurons were cross-linked with 1% formaldehyde diluted in neuronal culture medium (Neurobasal supplemented with B27, Glutamax and antibiotics) for 10 min at 37°C. Cross-linking was stopped by adding 125 mM glycine for 2 min at RT. After 3 PBS washes at 4°C, cells were lysed with Soft Lysis Buffer (50 mM Tris pH 8, 10 mM EDTA, 0,1% v/v NP-40 and 10% v/v glycerol supplemented with protease inhibitor cocktail (PIC; pepstatin, aprotinin, leupeptin and PMSF), followed by cell scrapping and centrifugation (3,000 rpm, 15 min at 4°C) for nuclear enrichment. Pellets were resuspended in SDS Lysis Buffer (1% v/v SDS, 10 mM EDTA, 50 mM Tris pH 8 supplemented with PIC). Then, chromatin was shredded by sonication using a BioRuptor Pico (Diagenode, cat no: B01060010; 10 cycles 30'' ON / 30'' OFF at 4°C), followed by centrifugation at 13,000 rpm for 10 min at 4°C. Supernatant-containing chromatin was recovered for protein quantification; 100 μg of protein were used by ChIP reaction. Of note, a 10% of each sample was saved as input. ChIP reactions were done using anti-H3K9me2 antibody (AbCam, mouse, #1220; 3 μg/reaction) and normalized to total Histone 3 (anti-H3, Millipore, #07-690, 3 μg/reaction) (reactions without antibodies were done as negative controls). Pre-cleared Protein A/G Agarose (Pierce-Thermo Scientific, #20422) was used for overnight immunoprecipitation at 4°C with agitation. Then, samples were washed 3 times with each of the following buffers: Low Salt (0,1% SDS, 1% v/v Triton X-100, 2 mM EDTA pH 8, 20 mM Tris pH 8 and 150 mM NaCl), High Salt (0,1% SDS v/v, 1% v/v Triton X-100, 2 mM EDTA pH 8, 20 mM Tris pH 8 and 500 mM NaCl) and LiCl buffer (250 mM LiCl, 1% v/v NP-40, 1% NaDOC, 1 mM EDTA and 10 mM Tris pH 8). After every wash, samples were centrifuged at 3,000 rpm for 3 min at 4°C. Supernatants were discarded and pellets resuspended in 100 μL of Elution Buffer (1% v/v SDS, 100 mM Na_2CO_3) for 30 min at 37°C. Then, samples were centrifuged at 11,000 rpm for 3 min and cross-links of IP eluates and input samples were reversed by adding 200 mM NaCl overnight (16-18 h) at 60°C. Finally, samples were treated with proteinase K for 1 h at 55°C (50 mM EDTA, 200 mM Tris pH 8, 100 μg/mL proteinase K). DNA was purified by phenol/chloroform extraction and precipitated at −20°C overnight with ethanol. DNA was resuspended in 50 μL of DNase/RNase free water. The promoter region of *Arhegf2* (−800 pb of TSS) was amplified by qPCR using SYBR Green master mix (Life Technologies), using the following primers Fw: ACAGAGAAATGG-GAGGCCTTG; Rv: AACATTTGAGCTCGCTGAGG. 4 μL of DNA were used for each qPCR. *Arhgef2* H3K9me2 levels are shown as the % of the input normalized by total H3 signal.

Imaging and post-imaging analysis

Imaging was done using a Zeiss LSM 800 confocal microscopy. FRET analyses were done using an Olympus IX81inverted microscope equipped with a DSU device, as previously described in FRET methods. Post-imaging analysis and quantifications were done in Fiji-ImageJ (NIH, USA).

QUANTIFICATION AND STATISTICAL ANALYSIS

Results are the mean ± standard error median (SEM) of at least 3 independent neuronal cultures. To check normal distributions, a Shapiro-Wilk test was applied before statistical procedures. For parametric distributions, a Student's t test or ANOVA was applied, whereas either Mann-Whitney's or Kruskal-Wallis's test for non-parametric. The number of biological replicates (N) from independent pregnant rats (for neuronal cultures) or mice (for IUE assays), are detailed in the corresponding figure legends. Asterisks in each figure represent significance level: *$p < 0.05$, **$p < 0,01$, ***$p < 0,001$, ns = non significant. Statistics and plots were done using GraphPad Prism 6.